Density fluctuations during crystallization of colloids

Klaus Schätzel
Institut für Angewandte Physik, Universität Kiel, D-2300 Kiel, Germany

Bruce J. Ackerson
Department of Physics, Oklahoma State University, Stillwater, Oklahoma 74078
(Received 20 November 1992)

Long-wavelength density fluctuations are recorded by small-angle light scattering during the crystallization of hard colloidal spheres. Measured structure factors show approximate scaling with a peak at finite scattering vectors. The time dependences of the peak intensity and the wave vector clearly reveal two different crystallization regimes. For samples near melting density, we find diffusion limited growth at small times and Lifshitz-Slyozov ripening at large times. Growth exponents in the ripening process seem to increase for higher densities. All measurements demonstrate a strong coupling of the observed conserved density parameter to the nonconserved crystal-order parameter.

PACS number(s): 64.70.Dv, 81.10.Fq, 82.70.Dd

I. INTRODUCTION

While the study of crystallization phenomena has a long history [1], our theoretical understanding of this important first-order phase transition is still rather poor. The very definition of a nonconserved order parameter "crystallinity" is not straightforward, if features like local crystal orientation are to be incorporated. Furthermore, solidification of atomic or molecular systems involves several additional conserved parameters: density, energy, and momentum. All these parameters will typically be coupled to the order parameter in a nonlinear fashion. In view of these complications, it is not surprising that most treatments of crystallization phenomena were based on phenomenological approaches, some of which will be outlined in Sec. I A.

Experimental investigations of crystallization kinetics are also sparse, particularly for solidification through homogeneous nucleation. Major problems in atomic systems are the high speed of nucleus formation and subsequent crystal growth as well as the difficulty of preventing heterogeneous nucleation under conditions of large supercooling [2]. Recent work on polymers [3] and model colloids [4–7], however, indicates a change of this situation. The dynamics of these systems proceeds sufficiently slowly to allow direct, time-resolved measurements of crystallization kinetics [7–10]. While these Brownian systems are not identical to atomic ones, because energy and momentum are not conserved due to their strong coupling to a suspending fluid, many of the essential features of the phase transition are. Furthermore, the smaller number of relevant parameters may even ease the task of theoretical modeling. In Sec. I B we will summarize previous work on colloidal crystallization.

A. Phenomenological theories

In the classical picture [11], solidification of atomic matter proceeds via nucleation and subsequent growth of small crystallites. The growth period is followed by a much slower ripening process, where large crystals grow at the expense of smaller ones.

Nucleation most often occurs through the presence of local impurities—as heterogeneous nucleation. Only in the absence of impurities is it possible to observe homogeneous nucleation, the spontaneous generation of crystal nuclei from thermal fluctuations [12]. Except at very large supercooling, homogeneous nucleation is typically associated with a large energy barrier. The favorable decrease of bulk energy in a small crystallite is more than offset by unfavorable surface tension contributions, unless the crystal size exceeds a certain critical diameter. Once beyond the critical size, further growth of the crystal proceeds extremely rapidly.

Characteristic of homogeneous nucleation is the dramatic dependence of the nucleation rate upon undercooling. Moderate temperature changes, say by 1% of the melting temperature, lead to order of magnitude changes in the nucleation rate. Such strong temperature dependences were indeed found experimentally, for example, by Turnbull's droplet technique [2], where the small volume of droplets limited the detrimental effects of impurities and of the rapid growth of nucleated crystals.

To our knowledge, there are no time-resolved studies of the growth following homogeneous nucleation in atomic matter. Crystal growth is typically studied at small undercooling for heterogeneously nucleated crystals, where the process proceeds sufficiently slowly for direct observation. In this situation, the incorporation of atoms into the growing crystal limits the growth rate and constant growth velocities are typical (interface limited growth). However, if there are composition differences between solid and liquid, diffusive processes may be rate limiting and square root of time growth laws are expected [13]. More complicated situations arise if heat transport away from the crystallization front is included in the analysis [14,15].

Late-stage ripening processes have achieved much recent attention for different first-order phase transition

processes [13]. Classical prototypes are the $t^{1/3}$ Lifshitz-Slyozov behavior found for systems with conserved order parameter [16] and the $t^{1/2}$ Lifshitz-Allen-Cahn behavior, which is characteristic for systems with nonconserved order parameter [17]. With crystallinity being nonconserved, one assumes the latter type of ripening should apply to solidification processes.

B. Colloidal crystals

Colloidal crystals are ordered, periodic structures of colloidal particles, which are suspended in a fluid. Popular systems are charged spheres, where particles repel each other by screened Coulomb potentials, and uncharged spheres, which interact predominantly just through hard-core repulsion. In both cases, there is no attractive interparticle force necessary to form crystals. For hard spheres entropic driving forces are sufficient to drive solidification at high densities [18–20].

Hard-core systems are special, since temperature is irrelevant for freezing. The density or the volume fraction, defined as the product of number density and single-particle volume, is the only available control parameter. Computer simulations as well as density functional theory yield freezing and melting volume fractions of 0.494 and 0.545, respectively [21]. By continuous compression it would be possible to increase the volume fraction up to the close packing limit $\pi/3\sqrt{2} = 0.74$. However, colloidal solids are typically prepared by rapid quenches from a metastable fluid phase. These quenches lead to glasslike amorphous phases for volume fractions in excess of 0.58 [22]. Such colloidal glasses cannot be compressed beyond the maximum random close packing volume fraction of 0.64 [23,24].

Several previous studies of colloidal crystals determined their phase diagrams and equilibrium structures [6,22]. For hard-sphere systems, the theoretical transition densities were well reproduced [25]. The final structure obtained by rapid quench experiments was found to be a random stacking of hexagonal layers, with just a small tendency to favor fcc packing at some volume fractions [26]. Microscopic observations of single crystals during growth indicated rounded, sometimes slightly "lozenge" shapes [22].

Previous kinetic measurements included video microscopy of single crystals and turbidity data for charged spheres, where growth with constant radial velocity was observed [4]. Dhont, Smits, and Lekkerkerker performed a series of time-resolved measurements on growing crystals of weakly charged particles [27]. They recorded the scattered light intensity around the first Bragg reflection and evaluated their data in terms of an "induction time," nucleation and growth rates, as well as numbers and sizes of nucleated crystals. On hard spheres, there exist a few observations of times since the quench, when crystals could first be seen by eye [28] and growth rates estimated from samples undergoing sedimentation [29]. In both cases the authors assumed a growth with constant radial velocity but did not actually prove this fact experimentally.

Some of these kinetic data were compared to theoretical expectations based upon the classical theory of nucleation and growth [30]. There was agreement on a qualitative level, but significant quantitative deviations were found between hard-sphere systems, soft-sphere systems, and the theoretical predictions. No nucleation rate data were included in this study, but later measurements on weakly charged spheres [7] clearly showed a much less dramatic dependence on density than what was predicted on the basis of classical nucleation theory.

None of the kinetic studies was extended into the late-stage ripening or coarsening phase of crystallization. Our small-angle light-scattering data, which were recently presented in a Letter [10] and will be described in detail here, appear to be the first observation of such a ripening on hard-sphere colloids. In addition we also obtained a wealth of new data on the early time nucleation and growth phase.

In the main part of this paper we present the experimental results of a series of small-angle light-scattering experiments during the crystallization of a model colloid, which closely approximates a hard-sphere system. Section II will describe our samples and the experimental setup. Kinetic small angle scattering data will be presented in Sec. III and Sec. IV will discuss our present interpretation of these data.

II. EXPERIMENT

A. Particles

All measurements reported here were performed on samples of polymethyl-methacrylate (PMMA) spheres, which were coated with a thin layer (some 10 nm) of hydroxystearic acid [31]. This coating provides sufficient steric stabilization to prevent flocculation. The particles were suspended in a mixture of decalin and tetralin, which closely matched the particles' index of refraction. Hence clear samples were obtained even at high volume fractions of the order of 50%. The difference in index of refraction between core and coating prevented a perfect index match of the particles. Such a perfect match also would have been difficult to maintain, due to its sensitivity to changes in sample temperature or probing wavelength. All our samples showed a total scattering of less than 50% of the incident light for a path length of 10 mm at a wavelength of 633 nm.

The particle radius was 500 nm as determined by dynamic light-scattering experiments on diluted samples. Polydispersity was estimated by static light scattering to be less than 5% relative standard deviation. For our comparatively large particles we observed very little tendency to grow heterogeneously nucleated crystals on the cell walls. However, sedimentation effects are quite marked. A free particle would sediment at a velocity of the order of 0.1 mm/h. This velocity is reduced by strong particle interactions in concentrated samples and significant sedimentation was not observed until after about one day [32].

Samples at different particle densities were prepared

three years ago [33]. The volume fractions were determined by careful weighting and drying of part of a stock solution, followed by controlled dilution with the prepared mixture of decalin and tetralin. Phase diagrams obtained from sedimentation studies on the samples three months after preparation were in reasonable agreement with theoretical calculations for hard-core systems, if a small correction (+3.6%) was made to all the measured volume fractions [32]. Such a correction may account for some swelling of the particles, most probably due to the finite solubility of tetralin in the hydroxistearic acid coating. This correction was smaller than the one reported by Pusey and van Megen on similar PMMA particles in decalin-CS_2 [25], most likely due to the larger diameter of our particles. Measurements of phase diagrams [25,34], sedimentation behavior [32], particle response to shear [35], and extremely small values of measured electrophoretic mobilities [36] all indicate that our PMMA particles closely approximate an ideal hard-core system.

Repeating the sedimentation experiments with our samples 14, 23, and 31 months after preparation, we noticed slight changes in their phase behavior. These changes were largely due to slow evaporation of some solvent (rates between 10 and 50 mg/year), which was detected by reweighting of the samples. We used this gradual increase in sample concentration to check the phase behavior of individual samples. As indicated in Fig. 1, the observed volume fractions of the crystalline phase as a function of density corresponded reasonably well to what is expected for hard spheres. In Fig. 1 each sample's density was rescaled (corrections between 2% and 7% as given in Table I) in order to obtain best fits to the theoretical hard-sphere phase diagram. Unfortunately, this procedure could not be applied to samples

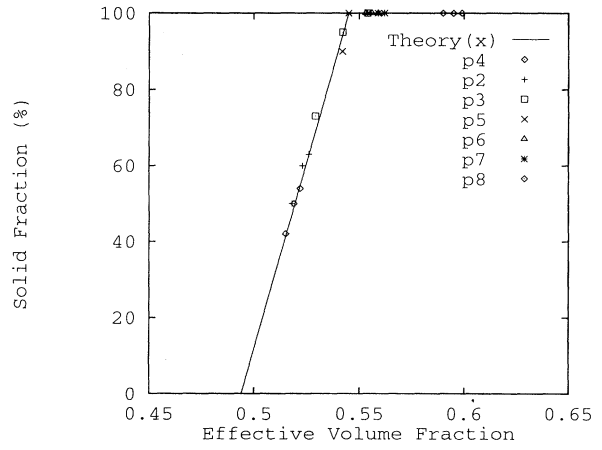

FIG. 1. Experimental phase diagram of our particle system as determined from measurements nine months before, at the time of our light-scattering measurements, and eight months later (increasing volume fractions). We show equilibrium solid fraction vs effective particle volume fraction. Sample P8 appeared to be glassy, all other samples formed small polycrystals. The theoretical prediction of the phase diagram for hard-core particles was taken from [21] (continuous line).

TABLE I. The sample volume fraction according to weight at the time of preparation, ϕ_i, at the time of the crystallization experiments, ϕ_w, and the volume fraction of the corresponding ideal hard-core system, ϕ_e. The accuracy of the last digit is doubtful.

Sample	P2	P3	P4	P5	P6	P7	P8
ϕ_i	0.443	0.462	0.474	0.482	0.492	0.501	0.523
ϕ_w	0.497	0.531	0.490	0.508	0.519	0.521	0.555
ϕ_e	0.523	0.542	0.519	0.545	0.556	0.559	0.595

already above melting density (our P6, P7, and P8), as for these fully crystalline or even glassy samples no phase boundary could be observed. In the case of P6 and P7, the method still sets a lower limit of about 6% for the necessary density corrections. We used—somewhat arbitrarily—the correction factor of sample P5 (7%) for all three higher density samples.

Table I gives the initially measured sample volume fractions ϕ_i at preparation, measured values ϕ_w based upon sample weights at the time of our light-scattering experiments, and the effective volume fractions ϕ_e, which we believe to characterize the ideal hard-core system which most closely matches the observed phase behavior of each individual sample.

Samples were transformed to a metastable amorphous state by shear melting [37]. Vigorous stirring was required to loosen up dense sediments, which typically formed at the bottom of all samples after a few days. Crystals could easily be melted by tumbling of the cuvettes at a rate between 10 and 20 revolutions per minute. After tumbling, samples were left at rest to crystallize. Due to the viscosity of the solvent (2.37×10^{-3} Pa s at 20 °C) all macroscopic flows stopped within a few seconds. Since crystallization occurred on a time scale of 10^3 s, the initial time ($t = 0$), where crystallization started, was well defined.

B. Small-angle light scattering

Static light scattering has typically been used at scattering angles close to the peak in the fluid structure factor or a low-order Bragg reflection of a colloidal crystal. For concentrated hard-sphere systems, this is also the region where the single-particle form factor falls from its low-angle limit of unity [22]. Our measurements, however, were all performed at much smaller scattering angles, where form factors and equilibrium structure factors are essentially constant. These light-scattering experiments on colloids are quite analogous to small-angle x-ray or neutron studies on atomic matter. We expect to probe density fluctuations on length scales large compared to particle diameter and spacing.

Low-angle scattering experiments demand special attention. They require the use of a wide beam with a narrow range of spatial frequencies. The number of optical surfaces should be kept as small as possible and all surfaces must be kept very clean to reduce stray light.

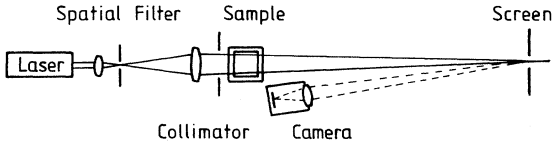

FIG. 2. Optical setup used for small-angle light scattering.

Our light-scattering setup (Fig. 2) utilized a small HeNe laser (5 mW, polarized). The beam was spatially filtered and expanded using a microscope objective (20×) and a pin hole (25-μm diameter) in a commercial mechanical unit (Newport). The resulting divergent beam was refocused with a single "best form" lens (f = 80 mm, antireflection coated for 633 nm). The expanded beam passed through a 9 mm circular aperture placed just before the sample, which limited the beam close to its first diffraction minimum. This kept low-angle scattering due to diffraction at this aperture sufficiently small. The use of a beam slightly narrower than the sample cell eliminated diffraction due to light propagating through the side walls of the cuvette.

After transversing the sample, which was contained in a rectangular cuvette (10 × 10 mm^2), the illuminating beam finally hit a distant screen about 1 m from the sample. A hole with a diameter between 2 mm and 5 mm was cut into the center of the screen to allow the primary beam to pass to a distant beam stop. Smaller holes were used for samples in the coexistence region, which produced strong scattering at very small angles. Larger holes were used for samples at higher densities, where the scattered intensity was weak but peaked at larger angles.

Scattered light was detected by a charge-coupled device (CCD) video camera placed slightly off axis, typically just below the main beam and close to the sample. This arrangement kept geometric distortions of the observed small-angle scattering pattern and possible influences of the scattering function of the screen negligible. The scale of scattering vectors q in the camera plane was calibrated by placing a grating of known spatial frequency in the position of the sample, typically using two orthogonal orientations of the grating. The camera resolved 192 by 165 pixels. All exposure times were kept close to 200 ms.

C. Data analysis

Image data were immediately digitized with 8-bit resolution and stored on magnetic disks. Frame rates varied between one image every 3 min at small times (after shear melting) and one image per hour at large times, typically. Data were processed on a personal computer. The processing involved careful manual centering of each series of scattering images followed by the calculation of radial intensity distributions $I(q)$. Most of the recorded images showed sufficient circular symmetry to justify this procedure.

The problem of static low-angle scattering by the cuvette and—typically much less—by the optical system was solved by subtracting an early image of each sequence from all the others. For most of our samples, the magnitude of the subtracted background was small compared to the recorded intensities at large times. At the same time, the subtraction procedure eliminated any constant offset (dark level) from the image data. The image of choice for background subtraction was typically the one with the smallest intensity data throughout the useful q range. In most cases all early images (less than 10 min from start of crystallization) were almost equivalent. But some experiments showed rapid small initial changes which we attribute largely to thermal equilibration of the sample, which becomes visible through the sensitive dependence of index matching on temperature.

The transmission of the samples was typically found to change by no more than 10% during the course of crystallization. We did not correct our data for these changes. The intensity of the observed small-angle scattering was well above multiple scattering contributions, as estimated from a consideration of double scattering.

Background corrected images typically showed rings, that is, the scattered intensity attained its maximum at some finite scattering vector. As a function of time, we observed a rapid growth of the scattered amplitude accompanied by a slow shift of the intensity peak towards smaller scattering vectors (Fig. 3). Hence data were evaluated in terms of position and height of the peak in the radial intensity distribution. Practical experience showed that the fit of a second-order polynomial to the $I(q)$ data around the peak provided a reasonable estimate of peak height I_m. The peak positions calculated from such a fit contained, however, large statistical errors due to noise on the scattering data. More stable scattering vector estimates were obtained by looking for the characteristic q value $q_{1/2}$ where the intensity beyond the peak had

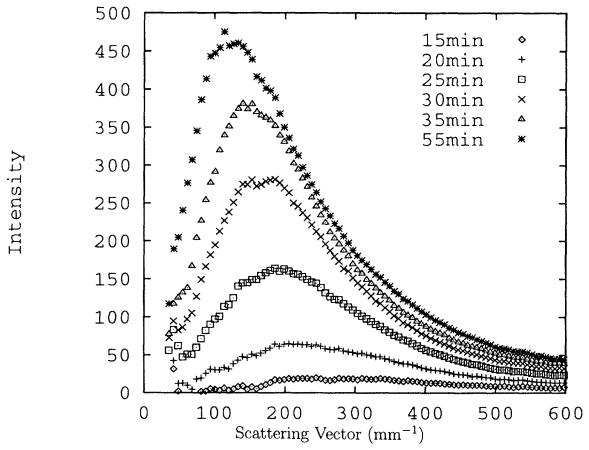

FIG. 3. Temporal evolution of measured light-scattering intensity as a function of scattering vector for sample P3. For comparison, the lowest-order Bragg peak is observed at scattering vectors larger than 6/μm, more than one order of magnitude larger than the peak in our low-angle data.

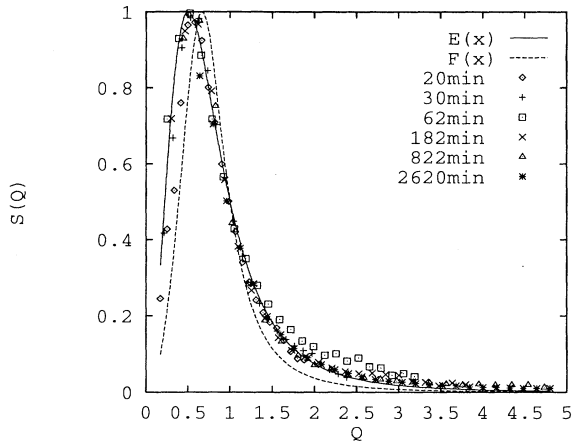

FIG. 4. Temporal evolution of scaled structure factors for sample P3. Empirical scaling function E(Q) (continuous line, see Sec. VI C) and Furukawa scaling function F(Q) [47] (broken line) are included for comparison.

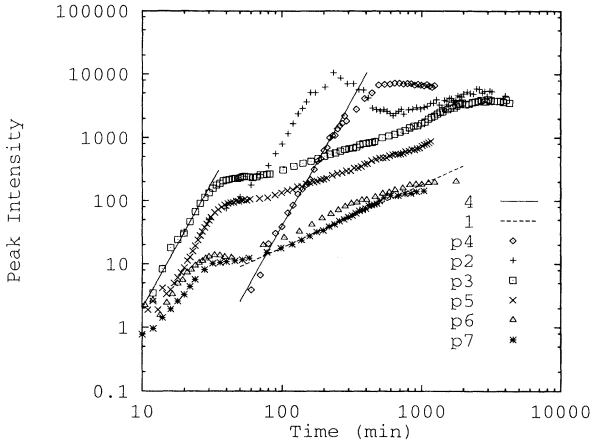

FIG. 5. Peak intensity $I_m(t)$ as a function of time t for samples P2–P7. Power laws t^4 (continuous line) and t^1 (broken line) are indicated.

fallen to $\frac{1}{2}$ of the peak value. I_m and $q_{1/2}$ were studied as functions of time and also used to obtain normalized structure factors

$$S(Q) = I(q)/I_m \quad , \quad Q = q/q_{1/2}. \tag{1}$$

As an example, Fig. 4 shows normalized structure factors obtained for sample P3, which was close to the melting volume fraction. Note the extraordinary range of times over which we observe scaling of these low-angle scattering data.

III. RESULTS

A. Time dependence

Since the normalized structure factors exhibit scaling, the data may be characterized by the two scaling parameters I_m and $q_{1/2}$. In order to discuss the time dependence of our light-scattering data, we plotted peak intensity I_m and characteristic scattering vector $q_{1/2}$ as functions of the time t elapsed since stopping the shear melting (Figs. 5 and 6). Double logarithmic scales were used to cover the large dynamic range of all our data. All intensities were represented on approximately the same scale, compensating for differences in the optical setups, apertures, and exposure times of individual experiments.

A prominent and common feature of $I_m(t)$ for all samples is the clear distinction of two very different phases of solidification. An initial phase, which is characterized by an intensity growth between t^3 and t^4, shows a sharp transition to a second process with a moderate, linear, or sublinear growth in peak intensity. Transition times are close to 30 min for sample densities close to melting or higher. Lower volume fraction samples show significantly larger crossover times.

For all samples investigated in the coexistence region, i.e., at densities up to melting, the initial rise of peak intensity as a function of time follows a t^4 law. Only the two higher density samples, P6 and P7, seem to indicate weaker growth, more like t^3. However, these samples also show the smallest total scattering intensities and our present data do not exceed the noise floor sufficiently in order to unambiguously prove a different growth law over a sufficient range of time.

The late-stage growth in peak intensity proceeds approximately proportional to t in samples P6 and P7. Samples P3 and P5, which were close to the melting density, indicate a slightly weaker growth. The lowest density samples P4 and P2 could not be measured for a sufficient length of time to detect their late-stage growth laws. This limitation arose due to significant interference by sedimentation under gravity.

In addition to the two power-law regimes at small and large times, a significant region of small intensity change or even a decrease in peak intensity with increasing time t was observed at intermediate times in samples P2 and P4.

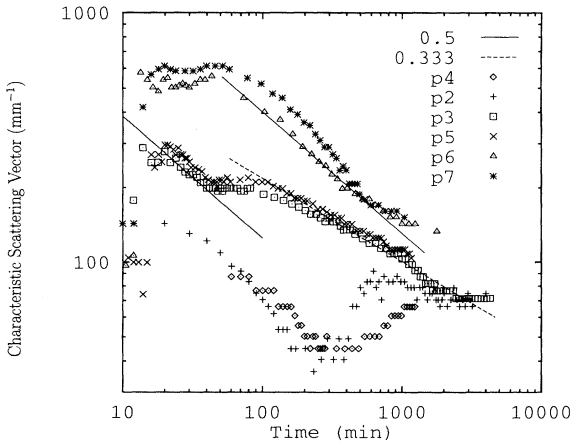

FIG. 6. Characteristic scattering vector $q_{1/2}(t)$ as a function of time t for samples P2–P7. Power laws $t^{-1/2}$ (continuous line) and $t^{-1/3}$ (broken line) are indicated.

The characteristic scattering vector as a function of time t (Fig. 6) shows a similar distinction into different time regimes as do the peak intensity data. The situation is particularly clear, again, for samples close to melting density (P3 and P5). At small times, the peak position moves as $t^{-1/2}$, there is no motion at intermediate times, and a slower motion like $t^{-1/3}$ at large times.

For samples at lower densities (P4 and P2), the small magnitude of the characteristic scattering vector made its precise determination difficult. The data point towards a slightly steeper decrease than $t^{-1/2}$ at small times and a peculiar increase at intermediate times.

Higher density samples (P6 and P7) reveal approximately constant characteristic scattering vectors throughout small and intermediate times and a clear decrease at large times. This decrease closely follows a $t^{-1/2}$ law for P6 while P7 data indicate an even slightly larger negative exponent.

Please note that the scattered data at small times ($t < 20$ min) are not significant. At these very early times, the peak in the structure factor at small scattering vectors q was not yet clearly above the noise floor and residual low-angle noise was likely to be taken for the peak. Data at intermediate times, where we observe little change of the characteristic scattering vector with time, possibly already fall into the crossover between the fast and slow processes, and we may well have missed a possibly existing regime of decreasing $q_{1/2}$ at very early times in our present measurements.

B. Scaling of the structure factor

In order to recognize changes in the shape of measured structure factors, we rescaled our raw data by peak intensity and characteristic scattering vector. Figure 4 already showed such data obtained for sample P3 through a large range of times. Early and late data seem to coincide almost perfectly. For times close to the onset of the late-stage growth process, we typically recognize a small skewing of the structure factor with a peak motion towards smaller scaled scattering vectors Q and slightly more weight in the large Q tail.

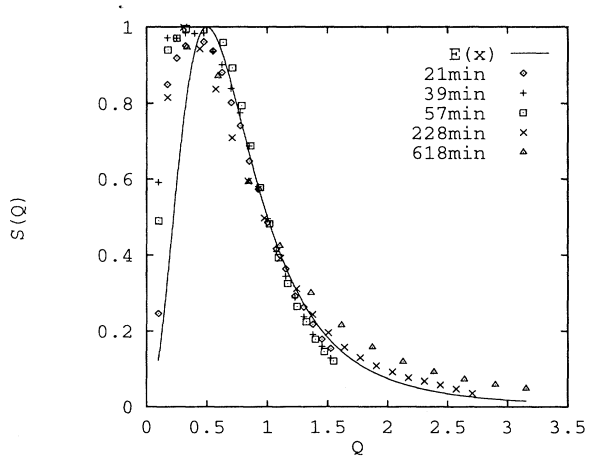

FIG. 7. Temporal evolution of scaled structure factors for sample P7 and empirical scaling function E(Q) (continuous line, see Sec. VI C). Deviations from scaling are visible, particularly at large times.

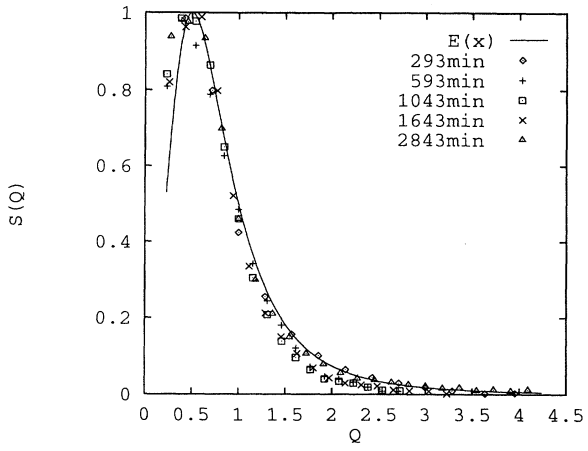

FIG. 8. Temporal evolution of scaled structure factors for sample P2 and empirical scaling function E(Q) (continuous line, see Sec. VI C).

While the behavior of sample P5 closely matches that of P3, the denser samples P6 and P7 show increasing deviations from perfect scaling. These deviations are most obvious for sample P7 (Fig. 7). At early times we find similar shapes as for the lower density samples with some downward motion of the large Q tail. However, during the late-stage growth we see definite skewing: The peak moves towards smaller Q and the tail rises significantly.

At lower sample densities, the absolute peak positions move towards smaller scattering vectors q and it becomes experimentally difficult to access scattered intensites at q values below the peak positions. This is evident in Fig. 8, which shows data obtained for sample P2. Within the limited accuracy of these data, no definite deviations from scaling were detected.

IV. DISCUSSION

A. Qualitative discussion

Previous structure factor data for order-disorder transitions were mostly obtained by measurements of the nonconserved order parameter. These structure factors always show a monotonic decay with increasing scattering vector; the largest signal is obtained at zero scattering vector [13]. In contrast, our data generally show a clear maximum of the scattered intensity at some finite scattering vector. We see "rings" qualitatively like those observed in spinodal decomposition [38,39], a process where the order parameter is conserved.

There is a fundamental reason for the observation of "rings." Small-angle light scattering is generated by long-wavelength density fluctuations in the sample. Initially

the sample had a uniform density. Since density is a conserved parameter and obeys diffusive transport, only finite wavelength density changes are achievable within any finite time. Hence our structure factors must strictly vanish at zero scattering vectors and attain their maximum at some finite scattering vector.

If we consider the formation of a single crystallite in a metastable fluid, the region of spontaneous crystal order will have reduced osmotic pressure, be compressed, and create a depletion zone having lower volume fraction in the surrounding (fluid) phase. The integrated densities exactly balance each other due to particle number conservation. Again there should be no scattering at very small scattering vectors, which correspond to extremely long-wavelength density fluctuations.

Actually we must expect diffusion to slowly spread the depletion zone and hence reduce the range of small scattering vectors, where we see the decrease of the structure factor towards zero. But as long as the growth of the crystal keeps up with the spreading of the depletion zone, the shape of the structure factor will remain constant [40]. We will just see a gradual contraction in scattering vector—scaling behavior. This is exactly the behavior we found for samples close to the melting density.

The growth of crystals must also be accompanied by a strong increase in the total scattered intensity under small angles. The intensity due to a single (small or nearly index matched large) spherical crystal rises like the sixth power of its radius. Correspondingly, all our data indicate a rapid initial increase in peak intensity. The levelling off of this intensity at some finite time indicates completion of the growth phase.

The fact that the shape of the measured structure factors for sample densities close to melting stays similar even beyond this completion time is quite surprising (see Fig. 4). At these large times we expect crystals to be in near contact and increasing in size via some ripening process. A depletion zone model for single crystal growth is no longer applicable. Apparently, the dense packing of crystals at this stage induces sufficient spatial density correlation between crystal grains of different orientations to reduce the very low-angle light scattering at very large times.

B. Small times

In the context of classical theories of crystallization, it is tempting to view the fast growth process as the nucleation and growth of discrete crystallites. For random positions of the nuclei, the measured scattered intensity should equal the averaged form factor of these crystallites. For very early times it seems reasonable to assume a constant rate of nucleation. Hence at any time t, light is scattered by crystallites, which were nucleated at some time τ, uniformly distributed between times 0 and t. This assumption leads to a total scattered intensity proportional to

$$I(q,t) = \int_0^t I_1(q, t-\tau)d\tau, \tag{2}$$

where $I_1(q,t)$ denotes the scattering by a single crystallite at time t after nucleation.

Our second assumption is that of a self-similar single-crystallite form factor,

$$I_1(q,t) = [R(t)]^6 F(qR(t)), \tag{3}$$

of characteristic size $R(t)$ and peak scattering intensity proportional to the sixth power of $R(t)$. This assumption appears to be well satisfied due to the close index matching of our samples [41]. If we further assume a power-law growth for $R(t)$,

$$R(t) = R_0 t^{\alpha}, \tag{4}$$

we obtain a raw scattered intensity

$$I(q,t) = \frac{1}{\alpha q^6 (qR_0)^{1/\alpha}} \int_0^{qR_0 t^{\alpha}} z^{5+1/\alpha} F(z) dz. \tag{5}$$

We proceed by introducing a scaled scattering vector

$$Q = qR_0 t^{\alpha}, \tag{6}$$

which leads to a scattered intensity

$$I\left(\frac{Q}{R_0 t^{\alpha}}, t\right) = \frac{R_0^6 t^{6\alpha+1}}{\alpha} \frac{1}{Q^{6+1/\alpha}} \int_0^{Q} z^{5+1/\alpha} F(z) dz. \tag{7}$$

While the $t^{-\alpha}$ scaling of the scattering vector was immediately expected, we can now also predict the time dependence of the peak intensity as $t^{6\alpha+1}$. Our data for samples P3 and P5 are clearly compatible with $\alpha = 1/2$. This is true for both the peak intensity as well as the characteristic scattering vector data. The intensity scaling of the lower density samples P2 and P4 leads to the same conclusion of square root of time growth. The time dependence of the characteristic scattering vector agrees well with $\alpha = \frac{1}{2}$ for P4, while the P2 data point to slightly larger values of α, but do so over a very small range of times, only.

For the higher density samples, we cannot detect any significant change of the characteristic scattering vector at early times and find a slightly weaker increase of peak intensity as a function of time. We may either conclude that α falls below $\frac{1}{2}$ or that our assumption of a constant rate of nucleation does not hold at the times considered. In fact, if nucleation stopped, $\alpha = \frac{1}{2}$ would imply a peak intensity proportional to $t^{6\alpha} = t^3$, very much like the observed values.

The finding of a square root of time growth for the crystallization of hard spheres is in conflict with previous observations on charged colloidal particles [4], where a linear growth had been found or assumed. But there is an important distinction between the crystallization of spheres with hard core and those with long-range interactions: The hard-core particle crystal density is some 10% above that of the corresponding liquid at coexistence, whereas this density difference appears to be small for charged spheres [42]. Without a significant change in density between crystal and liquid phases, there is no

need to diffuse particles over large distances and interface limited growth should prevail.

C. Large times

Understanding the short-time process as nucleation and growth, the completion of this process leaves the sample with an equilibrium fraction in the crystallized state. Beyond the corresponding completion time t_c the crystallized fraction of the sample should remain approximately constant. This behavior may in principle be tested by static light-scattering experiments in the region of the first Bragg peak. The area under this peak should remain constant over time. Such experiments are under preparation at our laboratory.

Small-angle light scattering, however, clearly reveals further changes in our samples. We view these changes as a coarsening or ripening process, where large crystals grow at the expense of smaller ones. Assuming again perfect scaling, as justified by our data except for the highest volume fraction sample P7, there emerge simple relations between a characteristic length scale R and the scattering properties. The characteristic scattering vector $q_{1/2}$ should decrease as $1/R$. The peak scattering power of a single crystallite should increase as R^6. The total number of scattering crystals should decrease as R^{-3}. This implies a peak intensity which increases as R^3.

Comparing our data with these predictions, we find a growth like

$$R \propto t^{1/3} \tag{8}$$

for samples P3 and P5, which are close to the melting density. Both the approximate $t^{-1/3}$ behavior of $q_{1/2}$ and the t behavior of the peak intensity are visible in Figs. 5 and 6.

In fact an exponent of $\frac{1}{3}$ is quite common in coarsening processes. But this exponent is generally associated with phase transitions, where the order parameter is conserved — known as Lifshitz-Slyozov ripening [16]. In our case, the primary order parameter "crystalline order" is clearly nonconserved. But, of course, we have a second conserved parameter, which is density. Apparently, this parameter controls the coarsening process. Such a behavior would not be surprising at sample volume fractions in the coexistence region of the phase diagram. Here we have a mixture of crystals and liquid, both of different density. Particularly at low crystalline volume fractions, the original Lifshitz-Slyozov theory should apply, where material must diffuse from small crystals through the liquid phase towards large crystals. Unfortunately, our present data sets do not include samples at densities in the lower coexistence region, and data close to 50% solid fraction (samples P2 and P4) do not extend to sufficiently large times due to sedimentation problems.

At higher sample densities, coarsening is characterized by an increasing temporal exponent. For sample P6 the observed behavior closely matches Lifshitz-Allen-Cahn behavior,

$$R \propto t^{1/2}, \tag{9}$$

as is expected for phase transitions with nonconserved order parameter [17]. However, this agreement may be accidental. P7, the slightly more dense sample, clearly showed violations of scaling and the $q_{1/2}$ data of this sample indicate an even larger exponent than $\frac{1}{2}$. Without any data between samples P5 and P6 we cannot rule out a continuous increase of the coarsening exponent from $\frac{1}{3}$ to $\frac{1}{2}$ and even larger values at still higher densities.

Coarsening processes have often been found to obey dynamical scaling at large times resulting in intensity patterns given by

$$I(q,t) = q_{1/2}^{-d}(t) F\left(\frac{q}{q_{1/2}(t)}\right), \tag{10}$$

where d denotes the dimensionality of the system [43,44,38,45,46]. In order to compare our data to this prediction of dynamical scaling, Fig. 9 displays the measured peak intensities as functions of the corresponding characteristic scattering vectors. Samples P3 and P5 clearly satisfy dynamical scaling for $d = 3$ dimensions at large times. However, samples P6 and P7 seem to indicate $d = 2$. Such a behavior would really be expected for a two-dimensional system only [45]. At present we can only speculate that this fact may result from the two-dimensional nature of grain boundaries.

In this context, please note again the observed lack of scaling of the structure factors measured for sample P7 at large times. Quite clearly, additional experimental data are required for a complete discussion of hard-sphere crystal coarsening at large times.

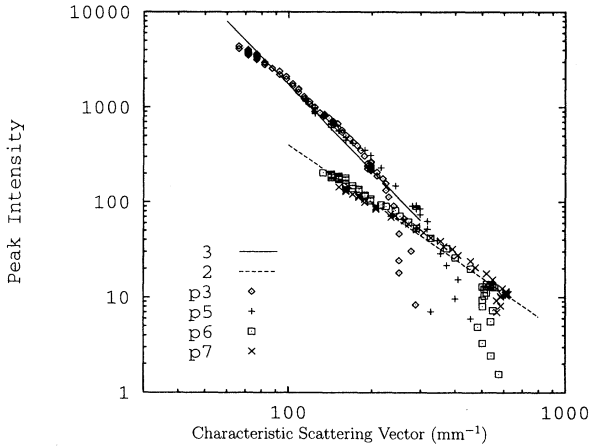

FIG. 9. Double logarithmic plot of peak intensity $I_m(t)$ as a function of characteristic scattering vector $q_{1/2}(t)$ for samples P3, P5, P6, and P7. A slope of -3 (continuous line) is expected based on dynamic scaling for three-dimensional systems. Large time data at high volume fractions are much closer to a slope of -2 (broken line).

D. Shape of the structure factor

Empirically it is possible to fit our structure factor data for samples and times where we observe good scaling by an expression

$$E(Q) = \frac{27Q^2}{2(1+2Q^2)^3}. \tag{11}$$

This function is similar to but distinctly broader than the Furukawa function

$$F(Q') = \frac{3Q'^2}{2+Q'^6}, \qquad Q' = 1.504Q, \tag{12}$$

which is valid for late-stage spinodal decomposition after off-critical quenches [47]. Both functions were included in Fig. 4.

At early times, we may consider the observed low-angle scattering to correspond to a single-crystal form factor. The density profile of a spherical crystallite surrounded by a diffusive depletion layer was calculated by Frank [40]. This calculation, however, leads to structure factors which are either much narrower than Eq. (11) or miss the peak position [48]. Assuming a very wide distribution of sizes of crystallites (say a negative exponential distribution) yields only moderate improvements. More efficient is the introduction of some nonspherical shape for the crystalites, e.g., a prolate ellipsoid [48]. Observations of aspheric crystals indeed were made on PMMA particle systems very similar to ours [22]. Some computer simulations suggest anisotropic nuclei, as well [49–51].

At late times, high solid fractions make single-crystal form factors an insufficient model for the observed scattering. An adequate treatment would have to include a structure factor contribution due to relative positions of individual crystals. The situation should approach a close packed system of nonspherical, polydisperse crystals at high solid fractions.

In view of these differences, it is even more surprising that for several samples, particularly close to the melting point, we observe essentially identical shapes of the measured structure factors from very early through very late times. The coincidence may well be accidental. However, please note the geometric similarity of an "early-time" depletion layer and a "late-time" grain boundary, both being essentially surfaces of crystals.

E. Density dependences

For a final discussion of our scattering data, we focus our attention upon the dependence of kinetic parameters on the volume fraction or density of our samples, the relevant control parameter. A characteristic time may — at least approximately — be defined as the crossover time or completion time of our small time process, t_c. A characteristic length may be defined as the size of crystals at this time t_c of the small time process. For spherical crystallites of radius R, calculations [48] yield a characteristic scattering vector

$$q_{1/2} \approx 1.8/R. \tag{13}$$

Let us use R_c to denote $1.8/q_{1/2}(t_c)$. While there remain some difficulties in defining this size for samples P2 and P4, which show a region of increasing $q_{1/2}$ close to t_c, the higher density samples allow a fairly unique definition of R_c. Figure 10 displays the characteristic crystal radii R_c as a function of density. We note a pronounced decrease towards larger densities, which may be extrapolated to almost zero at the glass transition density of 0.58 [52].

In addition to the usual explanation of glasses by complete freezing of the long-time self-diffusion, our data suggest a view of the colloidal glass as a solid where the grain size becomes comparable to the particle size. Still we need freezing of self-diffusion, however, in order to explain the absence of coarsening, which would lead to growing crystals at large times.

As shown by Russel [30], the classical theory of nucleation predicts enormous changes of nucleation rates for small changes of sample density. At the completion time t_c of the fast process, we can estimate the number density of crystals in each sample by the crystallized volume fraction divided by $(4\pi/3)R_c^3$, the typical volume of a single crystal. The ratio of this number density over the completion time may then serve as a rough measure of the nucleation rate. Figure 11 shows such nucleation rate estimates as a function of sample density together with Russel's prediction. Absolute nucleation rates agree well for samples P3 and P5. But the theoretically predicted density dependence is much stronger than what we observe experimentally. This disagreement sheds some doubt upon the applicability of a naive nucleation picture, where a large nucleation barrier must be crossed in order to generate a growing crystallite. Possibly, our crystallization experiments indicate a very moderate nucleation barrier only. We may even be close to a situation more like spinodal decomposition, where the phase transition starts spontaneously over a large range of wave vectors. This finding is supported by recent measurements

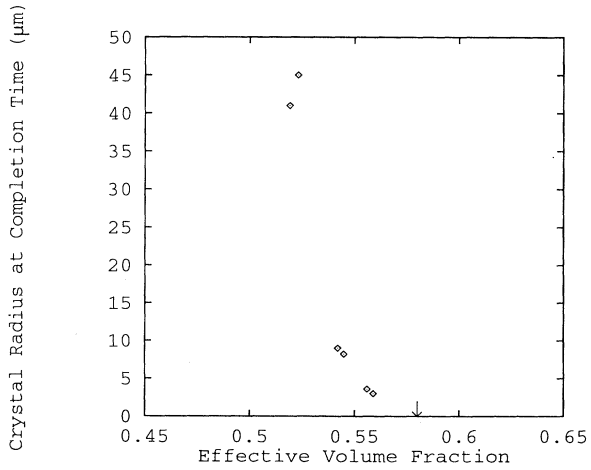

FIG. 10. Typical crystal radius R_c at completion time t_c as a function of effective particle volume fraction. The arrow denotes the volume fraction 0.58 beyond which samples remain in a glassy state.

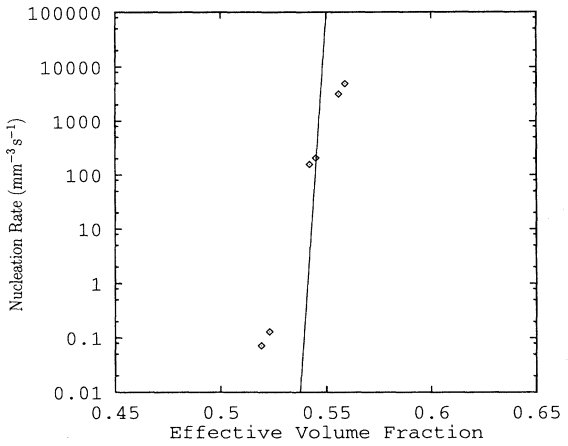

FIG. 11. Estimate of observed nucleation rates vs effective particle volume fraction. The continuous line corresponds to Russel's theoretical prediction [30].

of Dhont, Smits, and Lekkerkerker [27], who investigated the crystallization of slightly soft spheres by static light scattering close to the first Bragg peak. They also claim a much weaker dependence of nucleation rate on sample density than predicted by Russel.

The square root of time growth law found for our samples at small times leads to the definition of a growth coefficient of the same dimensions as a coefficient of diffusion. Hence it is tempting to plot this coefficient, approximated as R_c^2/t_c, in comparison to characteristic diffusion coefficients for hard-sphere systems. Figure 12 shows such a comparison with short- and long-time self-diffusion of single particles in the approximations used by Russel [30]. All data are normalized by the free particle diffusion coefficient. Collective diffusion would be slightly above 1 in this plot with little density dependence [22]. Our growth coefficient shows a sharp maximum in the upper coexistence range, where it clearly exceeds self-diffusion. It falls off much more rapidly than self-diffusion towards larger densities.

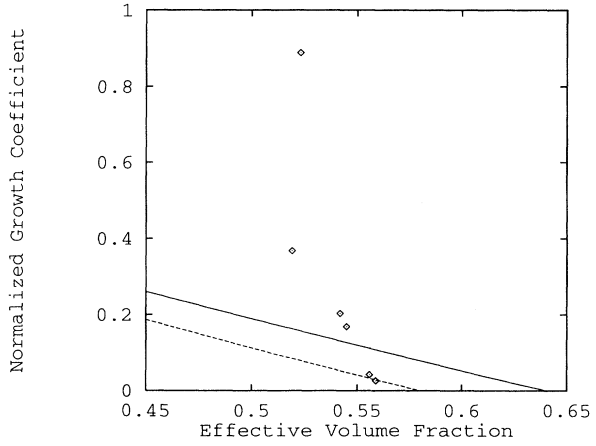

FIG. 12. Experimental growth coefficients R_c^2/t_c vs effective particle volume fraction. The continuous and broken lines are estimates of the short- and long-time values of the coefficient of self-diffusion in a hard-sphere system, respectively [30]. All coefficients are given in units of the free particle diffusion coefficient $D_0 = 0.19\ \mu\text{m}^2/\text{s}$.

F. Open questions

Our small-angle light-scattering measurements on the crystallization of hard-sphere colloids leave a number of questions open. Some of these questions are related to the nature of our samples. While the hard particle interaction potential seems to be a reasonable assumption, given the evidence presented in Sec. II A, the finite thickness of the polymer coating layer certainly implies some "softness" of the interaction if particles approach each other by distances less than 1/50 of a particle diameter. It remains to be studied what the consequences upon crystallization kinetics are — particularly at very high volume fractions.

Polydispersity is known to suppress crystallization if the relative standard deviation of particle size exceeds about 10% [22]. Experimental as well as theoretical studies are required in order to understand the effects of small polydispersities on phase behavior, crystallization kinetics, and relations to the glass transition. We plan to repeat some of our small-angle light-scattering studies on samples from different batches, which will be monitored for their polydispersities [53].

It is not yet experimentally verified what the actual levels of impurities are in our samples. Possible impurities may include small permanent clusters as well as a very small amount of particles with diameters significantly different from the mean diameter. While early photon correlation measurements on diluted samples indicated the presence of some impurities [54], more recent measurements performed with a cross-correlation setup to suppress multiple scattering [55,56] recognized the observed effects as artifacts due to residual double scattering [57]. Further experimental investigations using optical single-particle tracking [58] are under way. A different source of nucleation centers is possibly provided by our preparation of the metastable fluid state through shear melting. If this melting process did not completely destroy all crystalline order, this might well have profound consequences on crystallization kinetics. However, none of our samples appeared to be very sensitive to the actual conditions of shear melting such as shear rates and total times under shear.

A different class of open questions is provoked by our experimental results. As of yet, we have data at a few sample volume fractions only. In order to follow the indicated trends quantitatively, we need samples with closer and more precisely defined particle number densities. The use of just very few samples with densities that are modified through solvent evaporation seems to be the most promising approach.

Also we would like to extend the time range of our measurements. In order to cover smaller times, we need to reduce the low-angle flare of the apparatus, improve

the temperature stability of our setup, and increase the sensitivity of the detector. Towards large times, gravity induced settling presents a major problem. The use of smaller particles is a possible solution, time averaged zero gravity due to slow rotation of the sample may be another.

Within the time range of our present measurements, additional efforts will be required to improve the statistical accuracy of some of our data. Particular problems were noted at the crossover between the small and the large time regimes. Some of our data seem to indicate a dependence of the observed kinetics on beam height within the sample. Such early gravity dependence may be related to the first percolation of crystallites through the sample volume.

Finally it remains to point out once again the lack of adequate theories for crystallization kinetics in general, as well as for the particular process of hard-sphere crystallization in colloids.

V. CONCLUSIONS

Time-resolved small-angle light-scattering experiments on colloidal samples which closely approximate hard spheres yield intensities which peak at finite scattering vectors. The experiments clearly resolve two time regimes of the first-order phase transition from liquid to crystal.

The small time regime is characterized by a rapid growth in peak intensity and some decrease in peak position. It may be modeled by approximately constant homogeneous nucleation plus diffusive growth following a square root power law. Certainly none of our samples obeys a growth law with constant radial velocity.

The large time regime shows coarsening or ripening with length scales growing as $t^{1/3}$ for samples up to the melting point and larger exponents as $\frac{1}{2}$ or even more at higher sample densities. The character of this change in the growth law needs further investigation.

Through both regimes, samples around the melting point show good scaling to a common master function for which an empirical form may be given [Eq. (11)]. Attempts to explain the shape of this function lead to the suggestion that crystallites are nonspherical.

The density dependence of crossover times and the corresponding crystal size may be extracted and used to estimate nucleation rates. These estimates show much less dependence on density than expected from classical nucleation theory. Crystal sizes may be extrapolated towards larger sample densities and seem to approach zero close to the glass transition.

ACKNOWLEDGMENTS

The authors thank W. van Megen for useful discussions. Thanks to A. Heymann, T. Palberg, and H. Löwen for critical reading of this manuscript. We thank the Department of Energy for support through Grant No. DE-FG05-88ER45349 to B.J.A. K.S. received support from the Deutsche Forschungsgemeinschaft.

[1] D. B. Fahrenheit, Philos. Trans. R. Soc. London **39**, 78 (1724)..
[2] D. Turnbull, J. Chem. Phys. **20**, 411 (1952).
[3] C. R. Harkless, M. A. Singh, S. E. Nagler, G. B. Stephenson, and J. L. Jordan-Sweet, Phys. Rev. Lett. **64**, 2285 (1990).
[4] D. J. W. Aastuen, N. A. Clark, L. K. Cotter, and B. J. Ackerson, Phys. Rev. Lett. **57**, 1733 (1986); **57**, 2772 (1986).
[5] T. Okubo, J. Chem. Phys. **87**, 3022 (1987).
[6] Phase Transitions **21** (27) (1990).
[7] C. Smits, Ph.D. thesis, Utrecht University, 1991 (unpublished).
[8] D. J. W. Aastuen, N. A. Clark, J. C. Swindal, and C. D. Muzny, Phase Transitions **21**, 139 (1990).
[9] C. Smits, J. S. van Duijneveldt, J. K. G. Dhont, H. N. W. Lekkerkerker, and W. J. Briels, Phase Transitions **21**, 157 (1990).
[10] K. Schätzel and B. J. Ackerson, Phys. Rev. Lett. **68**, 337 (1992).
[11] J. Frenkel, *Kinetic Theory of Liquids* (Oxford University Press, Oxford, 1946).
[12] K. F. Kelton, in *Solid State Physics: Advances in Research and Applications*, edited by E. Reich and D. Turnbull (Academic, New York, 1991), Vol. 45, p. 75.
[13] J. D. Gunton, M. San Miguel, and P. S. Sahni, in *Phase Transitions and Critical Phenomena*, edited by C. Domb and L. Lebowitz (Academic, New York, 1983), Vol. 8, p. 269.
[14] S. A. Schofield and D. W. Oxtoby, J. Chem. Phys. **94**, 2176 (1991).
[15] H. Löwen, J. Bechhoefer, and L. S. Tuckerman, Phys. Rev. A **45**, 2399 (1992).
[16] I. M. Lifshitz and V. V. Slyozov, J. Phys. Chem. Solids **19**, 35 (1965).
[17] S. M. Allen and J. W. Cahn, Acta Metall. **27**, 1085 (1979).
[18] T. V. Ramakrishnan and M. Yussouff, Phys. Rev. B **19**, 2775 (1979).
[19] A. D. J. Haymet and D. Oxtoby, J. Chem. Phys. **74**, 2559 (1981).
[20] M. Baus, Mol. Phys. **50**, 543 (1983).
[21] W. G. Hoover and F. H. Ree, J. Chem. Phys. **49**, 3609 (1968).
[22] P. N. Pusey, in *Liquids, Freezing and the Glass Transition*, edited by D. Levesque, J. P. Hansen, and J. Zinn-Justin (Elsevier, Amsterdam, 1990).
[23] J. D. Bernal, Proc. R. Soc. London, Ser. A **280**, 299 (1964).
[24] N. E. Cusack, *The Physics of Structurally Disordered Matter: An Introduction* (Hilger, Bristol, 1987), Chap. 2.
[25] P. N. Pusey and W. van Megen, Nature (London) **320**, 340 (1986).
[26] P. N. Pusey, W. van Megen, P. Bartlett, B. J. Ackerson,

J. G. Rarity, and S. M. Underwood, Phys. Rev. Lett. **63**, 2153 (1989).
[27] J. K. G. Dhont, C. Smits, and H. N. W. Lekkerkerker (unpublished).
[28] P. N. Pusey and W. van Megen, in *Complex and Supramolecular Fluids*, edited by S. A. Safran and N. A. Clark (Wiley Interscience, New York, 1987), p. 673.
[29] K. E. Davis and W. B. Russel, Ceramic Trans. **1B**, 693 (1988).
[30] W. B. Russel, Phase Transitions **21**, 127 (1990).
[31] L. Antl, J. W. Goodwin, R. D. Hill, R. H. Ottewill, S. M. Owens, S. Papworth, and J. A. Waters, Colloids Surfaces **17**, 67 (1986).
[32] S. E. Paulin and B. J. Ackerson, Phys. Rev. Lett. **64**, 2663 (1990).
[33] S. E. Paulin, M.S. thesis, Oklahoma State University, 1989 (unpublished).
[34] B. J. Ackerson, J. Rheol. **34**, 553 (1990).
[35] B. J. Ackerson and T. A. Morris, in *Ceramic Powder Science III*, edited by G. L. Missing, S. Hirano, and H. Hausner (American Ceramic Society, Westerville, OH, 1990), Vol. 12, p. 349.
[36] W. Weise (unpublished)
[37] B. J. Ackerson and N. A. Clark, Phys. Rev. Lett. **46**, 123 (1981).
[38] T. Hashimoto, M. Itakura, and H. Hasegawa, J. Chem. Phys. **85**, 6118 (1986).
[39] T. Hashimoto, M. Itakura, and N. Shimidzu, J. Chem. Phys. **85**, 6773 (1986).
[40] F. C. Frank, Proc. R. Soc. London, Ser. A **201**, 586 (1950).
[41] M. Kerker, *The Scattering of Light* (Academic, New York, 1969).
[42] B. R. Laird and D. M. Kroll, Phys. Rev. A **42**, 4810 (1990).
[43] J. L. Lebowitz J. Marro, and M. H. Kalos, Acta Metall. **30**, 297 (1982).
[44] P. A. Rikvold and J. D. Gunton, Phys. Rev. Lett. **49**, 286 (1982).
[45] P. Wiltzius and A. Cumming, Phys. Rev. Lett. **66**, 3000 (1991).
[46] M. Carpineti and M. Giglio, Phys. Rev. Lett. **68**, 3327 (1992).
[47] H. Furukawa, Physica A **123**, 497 (1979).
[48] B. J. Ackerson and K. Schätzel, in *Complex Fluids*, edited by L. Garrido (Springer, Heidelberg, 1992), p. 15.
[49] M. J. Mandell, J. P. McTague, and A. Rahman, J. Chem. Phys. **66**, 3070 1977).
[50] J. N. Cape, J. L. Finney, and L. V. Woodcock, J. Chem. Phys. **75**, 2366 (1981).
[51] W. C. Swope and H. C. Andersen, Phys. Rev. B **41**, 7042 (1990).
[52] B. J. Ackerson, W. van Megen, and K. Schätzel (unpublished).
[53] W. van Megen (private communication).
[54] U. Nobbmann, M.S. thesis, Oklahoma State University, 1991 (unpublished).
[55] M. Drewel, J. Ahrens, and U. Podschus, J. Opt. Soc. Am. A **7**, 206 (1990).
[56] K. Schätzel, J. Mod. Opt. **38**, 1849 (1991).
[57] A. Heymann (private communication).
[58] K. Schätzel, W.-G. Neumann, J. Müller, and B. Materzok, Appl. Opt. **31**, 770 (1992).